

Catalysis Science & Technology

Accepted Manuscript



This article can be cited before page numbers have been issued, to do this please use: H. Abdullah, D. Kuo and N. S. Gultom, *Catal. Sci. Technol.*, 2019, DOI: 10.1039/C9CY00502A.



This is an Accepted Manuscript, which has been through the Royal Society of Chemistry peer review process and has been accepted for publication.

Accepted Manuscripts are published online shortly after acceptance, before technical editing, formatting and proof reading. Using this free service, authors can make their results available to the community, in citable form, before we publish the edited article. We will replace this Accepted Manuscript with the edited and formatted Advance Article as soon as it is available.

You can find more information about Accepted Manuscripts in the [author guidelines](#).

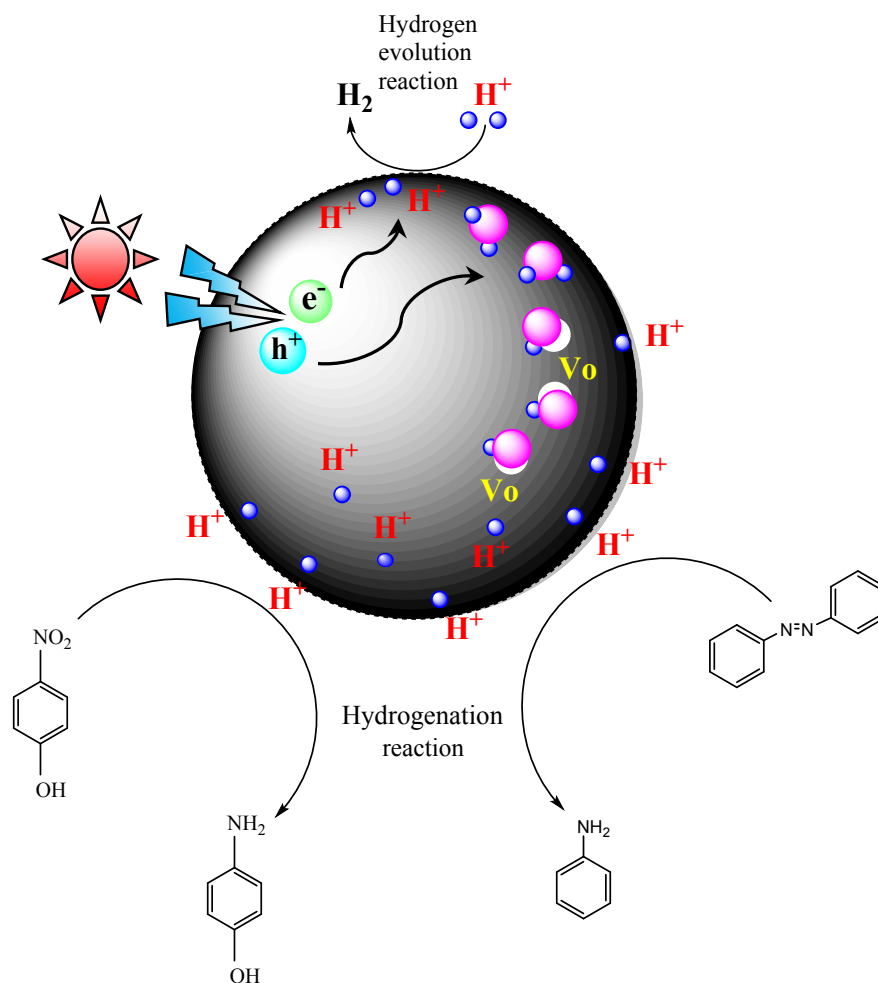
Please note that technical editing may introduce minor changes to the text and/or graphics, which may alter content. The journal's standard [Terms & Conditions](#) and the ethical guidelines, outlined in our [author and reviewer resource centre](#), still apply. In no event shall the Royal Society of Chemistry be held responsible for any errors or omissions in this Accepted Manuscript or any consequences arising from the use of any information it contains.

N=N bond cleavage of azobenzene *via* photocatalytic hydrogenation with Dy-doped Zn(O,S): The progress from hydrogen evolution to green chemical conversion

Hairus Abdullah, Dong-Hau Kuo*, Noto Susanto Gultom

Department of Materials Science and Engineering, National Taiwan University of Science and Technology, No.43, Sec. 4, Keelung Road, Taipei 10607, Taiwan

*Fax: +011-886-2-27303291. E-mail: dhkuo@mail.ntust.edu.tw

23 **Graphical Abstract:**

31 ABSTRACT:

32 Hydrogen-evolved Dy-doped Zn(O,S) photocatalyst with different amounts of Dy precursor has
33 been synthesized, characterized and further utilized for hydrogenation reactions. The Dy-
34 catalysts are firstly examined with electrochemical impedance spectroscopy, photo responsivity,
35 and hydrogen evolution reaction. Dy-Zn(O,S) with 10% Dy precduror shows the best
36 photocatalyst performance with a highest H₂ production rate of 8.160 mmol/g·h. This catalyst is
37 chosen for conducting the hydrogenation reaction. It is our intention to confirm the
38 correlationship between photocatalytic H₂ production rate and hydrogenation reactions of 4-
39 nitrophenol to 4-aminophenol and azobenzene to aniline, which is a step further in the
40 hydrogenation reaction to challenge the N=N bond cleave of azobenzene. A 100% photo
41 conversion of 60 ppm azobenzene to aniline in 6 h was confirmed under a low power UV light
42 illumination in a 10% ethanol solution. Kinetic steps and kinetic mechanism are proposed, which
43 involve the important reaction steps of solvation, adsorption, pinning, and surface hydrogenation
44 reaction to operate together.

45

46

Introduction

Nowadays, energy and environmental issues have emerged as important topics at global level. As fossil fuel has been the main source of energy, our society depends on fossil fuel for most of their activities. However, the process to obtain the energy from fossil fuel releases CO₂ to atmosphere and generates other environmental problems. The amount of CO₂ in air has significantly increased and caused the elevation of global temperature. Therefore, naturally obtained energy carriers are urgently required to lower the negative effects of energy harnessing to environment. One of the most fascinating works to alleviate the global warming effects is the research on hydrogen evolution. Hydrogen as one of the most efficient and clean energy carriers has a great potential to replace fossil fuel in the future for its harmless combustion product of water.¹ There are many reports on metal oxide, sulphide, phosphide, and oxysulfide solid solution photocatalysts for efficient photocatalytic water splitting using sacrificial reagents (such as Na₂SO₃, ethanol, and ethanolamine) in the past several decades.²⁻⁶ Photocatalysis with different kinds of semiconductor materials have been identified as one of the great methods to produce hydrogen due to its simplicity in applications, by which hydrogen can be generated with simply mixing semiconductor powders in water solution under the illumination with light.

Chemical conversion with photocatalytic hydrogenation reaction (PHR) is also an on-going issue for the green technology.⁷ It is an important fundamental of chemistry to promote environment-friendly chemical conversion for synthesizing useful substances. The application using TiO₂ semiconductor as a photocatalytic oxidant for detoxifying harmful chemicals has been avidly studied, because the photo-generated OH• radical can oxidize many organics.⁸ For photocatalytic reduction reaction, the efficient conversion of the toxic 4-nitrophenol (4-NP) to a

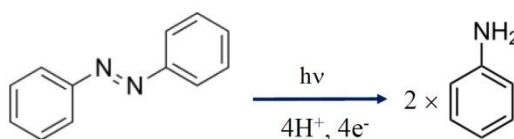
70 useful 4-aminophenol (4-AP) chemical with the Zn(O,S)-based nanoparticles without using
71 reducing agents had been successfully developed in our group, following the success in HER.^{7, 9,}
72 ¹⁰ For most of works on the 4-NP-to-4-AP conversion, ammonium formate and sodium
73 borohydrate as proton sources were applied to accelerate the reduction reaction.^{1,19} The
74 advantage of using our photocatalyst for liquid phase hydrogenation is the reaction cleanness and
75 safeness due to the in-situ proton generation for HER and chemical conversion. Therefore, PHR
76 of Zn(O,S)-based catalyst is promising and encouraging for further exploration to widen its
77 environment-friendly application.^{1, 9, 11-13}

78 Aniline is one of the most important intermediates for polyurethane, dyestuffs and
79 pharmaceuticals in industries.¹⁴⁻¹⁸ Currently, aniline production involves two steps, where
80 benzene is firstly nitrated with a concentrated mixture of nitric acid and sulfuric acid at 50-60 °C
81 to yield nitrobenzene (NB), followed by the catalytic hydrogenation at 200–300 °C.¹⁹ The NB-
82 to-aniline reaction also occurs at 90-125 °C under high H₂ pressure,²⁰⁻²² at 50 °C and H₂ pressure
83 of 3 MPa in ionic liquid,²³ and at 25 °C with electrocatalysis.²⁴ For PHR, NB also can be
84 converted to aniline over Bi₂MoO₆ with (NH₄)₂C₂O₄ as reducing agent or over g-C₃N₄ at 80 °C
85 with N₂H₄·H₂O in water.^{23, 25} Similar to the 4-NP-to-4-AP reaction, the NB-to-aniline one at a
86 mild condition also needs the strong reducing agent to provide protons.

87 Azobenzene (AB) with the N=N bond is a model chemical for the carcinogenic azo dyes
88 widely used in textile industries. While aniline is mainly synthesized from nitrobenzene, its
89 formation from AB by photocatalysis is less reported. Tada et al. in 2000 used Pt/TiO₂ catalyst to
90 complete the first study for the photocatalytic reduction of azobenzene.²⁶ Their rate of reduction
91 of AB to hydrazobenzene (HAB) increased with the loading of Pt to reach ~100% conversion,

91% selectivity for HAB, and 9% for aniline after 1h reaction. The amount of aniline increased to 19.2% after 3h reaction. Shiraishi et al. in 2018 reported PHR of AB had 95% selectivity for HAB and 5% for aniline.²⁷ At this stage, HAB remains the predominant product for the PHR of AB, although Density Functional Theory (DFT) calculation indicates that, in the gas phase reaction, the formation of aniline on catalyst by the reaction with AB in the presence of a source of hydrogen is energetically favored.

The present work intends to demonstrate that Dy-doped Zn(O,S) nanoparticles (NPs) with the photocatalytic HER capability can be used for the green chemical conversion through PHR. Two kinds of photocatalytic chemical conversions are selected: one is the conversion of 4-NP to 4-AP with sodium sulfate as a hole scavenger and the other is the conversion of AB to aniline with 10% ethanol in aqueous solution. The total AB-to-aniline reaction can be expressed as:



Zn(O,S) with different Dy contents were characterized and tested at the first stage to find the best composition for the photocatalytic chemical conversions at the second stage. A complete conversion of AB to aniline had been achieved. The photocatalytic activities of Dy-doped Zn(O,S) for the hydrogenation of nitro and azo groups were evaluated and elucidated with proposed mechanism.

Experimental Methods

Materials.

110 Zinc acetate dihydrate and dysprosium acetate hydrate were purchased from Alfa Aesar and
111 Sigma Aldrich, respectively. Thioacetamide (TAA) as a sulfur source was obtained from
112 Shanghai Aladdin Bio-Chem Technology Co., LTD. Hydrazine monohydrate ($\text{N}_2\text{H}_4 \cdot \text{H}_2\text{O}$) was
113 provided by Fisher Scientific U.K. limited. 99% 4-nitrophenol and 97%+ azobenzene were
114 purchased from Alfa Aesar and Acros Organics, respectively. Sodium sulfite anhydrous
115 (Na_2SO_3) was purchased from Alfa Aesar. All the chemicals were analytical grade without
116 further purification.

117 **Synthesis of Dy-doped Zn(O,S) NPs.**

118 Dy-doped Zn(O,S) powders were prepared based on the previous work¹ with different amounts
119 of $\text{Dy}(\text{CH}_3\text{COO})_3 \cdot x\text{H}_2\text{O}$ precursor at 0%, 5%, 10%, and 20% for samples of Dy-Zn(O,S)-0, Dy-
120 Zn(O,S)-5, Dy-Zn(O,S)-10, and Dy-Zn(O,S)-20, respectively. In a typical preparation for Dy-
121 Zn(O,S)-10 NPs, 20 mmol $\text{Zn}(\text{Ac})_2$ dihydrate and 2 mmol $\text{Dy}(\text{CH}_3\text{COO})_3 \cdot x\text{H}_2\text{O}$ were first
122 dissolved in 500 mL distilled water, then followed by adding 10 mmol TAA. The solution was
123 stirred to totally dissolve all the precursors, followed by heating to 95 °C with the ramp of 1.5
124 °C/min. After the solution temperature reached 95 °C, 0.5 mL $\text{N}_2\text{H}_4 \cdot \text{H}_2\text{O}$ was added into the
125 solution and continuously stirred for 4 h. Finally, the obtained white precipitate was collected by
126 centrifugation after washing for three times with alcohol. To remove all the volatile species, the
127 white powder was dried at 70 °C for 12 h in vacuum oven. The other catalyst powders for 0%,
128 5%, and 20% were prepared by the same experimental procedure with an appropriate amount of
129 $\text{Dy}(\text{CH}_3\text{COO})_3 \cdot x\text{H}_2\text{O}$.

130 **Characterization techniques.**

Morphology and microstructure of catalyst powder were both examined with field emission scanning electron microscopy (FE-SEM, JSM 6500F, JEOL, Tokyo, Japan). Powder X-ray diffraction (XRD) patterns of Dy-Zn(O,S) NPs with different contents of Dy precursor were recorded by Bruker D2-phaser diffractometer using Cu K α radiation with a wavelength of 1.5418 Å. Optical properties of Dy-Zn(O,S) NPs were examined with diffuse reflectance spectra (DRS) measurement using a Jasco V-670 UV-visible-near IR spectrophotometer. Energy bonding of each element in Dy-Zn(O,S) NPs was examined with X-ray photoelectron spectroscopy (XPS) measurement which was carried out on a VG ESCA Scientific Theta Probe spectrometer system with Al K α (1486.6 eV) source. Electrochemical impedance spectroscopy (EIS) measurement was conducted by using a Bio-Logic Science Instruments with EC-Lab® software. Glassy carbon electrode (GCE), Ag/AgCl electrode, and platinum plate were respectively used as the working, reference, and counter electrodes in an electrochemical cell. High performance liquid chromatography (HPLC, Shimadzu LC-2010AHT) measurement was used to ensure the conversion of 4-NP to 4-AP after photo reaction with each time interval of one hour. The reaction solution was detected with UV detector at the monitoring wavelength of 323 nm and with fluorescence detector at the emission and excitation wavelengths of 300 nm and 323 nm, respectively. The 4-NP and 4-AP in aliquots were examined with ODS Hypersil (C18) 250*4.6 column. The mobile phase was 20% methanol solution containing 5 mM tetrabutylammonium phosphate with the flowing rate of 1 mL/min at room temperature. To differentiate the azobenzene and aniline in aliquots, the reaction solution was collected and analyzed with Jasco V-670 UV-visible-near IR spectrophotometer and GC-MS with flame ionization detector (FID).

Photocatalytic HER experiment.

153 The capability of Dy-Zn(O,S) to evolve hydrogen was tested in 500 mL borosilicate reactor
154 containing 450 mL solution with 10% ethanol as a hole scavenger reagent. To evaluate the HER,
155 100 mg Dy-Zn(O,S) powders with different amounts of Dy were applied and the experiments
156 were run for 5 h with $4\text{ W} \times 4$ blacklight UV tube lamps (0.088 mW/cm^2) illumination. The
157 experiments were done with vigorous stirring to prevent the precipitation of catalyst powder
158 during the photocatalytic session. Prior to starting the HER experiment, the reactor which
159 containing catalyst-dispersed ethanol solution was purged by Ar with flowing rate of 100
160 mL/min for 1 h to remove all the atmospheric air in reactor. The existences of atmospheric air in
161 reactor were then evaluated with GC. If the signals from oxygen and nitrogen appeared in GC
162 analysis, the purging process had to continue. After the air in reactor had been sterilized, the
163 illumination system would be turned on and an aliquot was taken every 30 min. The sampling
164 process needed several minutes to flow the evolved hydrogen from reactor to GC system set with
165 the retention time of 0.6 min. Finally, the hydrogen amount was measured based on the peak
166 area.

167 **Photocatalytic hydrogenation of 4-NP to 4-AP.**

168 The hydrogenation of 4-NP experiment was conducted in a 500 mL reactor which was inserted
169 with $4\text{ W} \times 4$ UV blacklight lamps during the photocatalytic session. The reactor was
170 continuously flushed with Ar gas during reaction. In the experiment, 200 mg Dy-Zn(O,S)
171 powder was well dispersed in 450 mL 4-NP solution (30 ppm) containing 100 mg Na_2SO_3 . Prior
172 to starting the light illumination, the solution was stirred in dark condition for 30 min. An aliquot
173 was taken before the light illumination. After starting the light illumination, aliquots were taken
174 at the time interval of 15 min to easily observe the 4-NP conversion with UV-vis spectroscopy.

175 To ensure the total conversion of 4-NP to 4-AP, another experiment with the same condition was
176 carried out for 2 h with the aliquots were hourly taken. The aliquots were examined with HPLC
177 to ensure the conversion product of 4-AP. UV detector with the monitoring wavelength of 323
178 nm for detecting 4-NP and fluorescent detector with the excitation and emission wavelengths at
179 300 nm and 323 nm, respectively, for 4-AP were used during the HPLC measurement.

180 **Photocatalytic hydrogenation of azobenzene to aniline.**

181 The hydrogenation reaction for 15 ppm AB was also carried out in the same reactor as used for
182 the 4-NP reduction reaction. During the experiment, Ar gas was continuously flowed through the
183 reactor. To convert azobenzene to aniline, 200 mg catalyst powder and and 15 ppm AB were
184 dispersed in 400 mL aqueous solution with 10% ethanol. Ethanol was necessary not only for the
185 dissolution of azobenzene but also for being a hole scavenger reagent during PHR. To reach the
186 adsorption and desorption equilibrium between catalyst and azobenzene, the catalyst-dispersed
187 azobenzene solution was stirred for 30 min before starting the light illumination. Aliquots were
188 taken with a certain time interval before and during photocatalytic session and examined with
189 UV-vis spectroscopy. To further ensure the conversion product of aniline, GC-MS with flame
190 ionization detector (FID) was used to analyzed the product from the reaction with 60 ppm AB of
191 much high concentration.

192 **Results and discussion**

193 **X-ray diffraction (XRD) structure analysis.**

194 [Fig. 1](#) shows the XRD crystal structure of Dy-Zn(O,S) powders prepared with different Dy
195 precursor contents. XRD pattern of Dy-free Zn(O,S)-0 agreed with our previous work¹, with the

standard JCPDS files of ZnO and ZnS evaluated in Fig. S1 in supplementary data. The main peaks of Zn(O,S)-0 solid solution in the planes of (111), (220), and (311) were located between those of cubic ZnO (JCPDS #65-2880) and ZnS (JCPDS #05-0566). With increasing the Dy contents, XRD patterns of Dy-Zn(O,S) did not show the peak shifts, which indicated Dy-Zn(O,S) still remained solid solution with Dy embedded at the cation site. The average crystalline size of all Dy-Zn(O,S), calculated with the (111) peak, was about 2.5 nm.

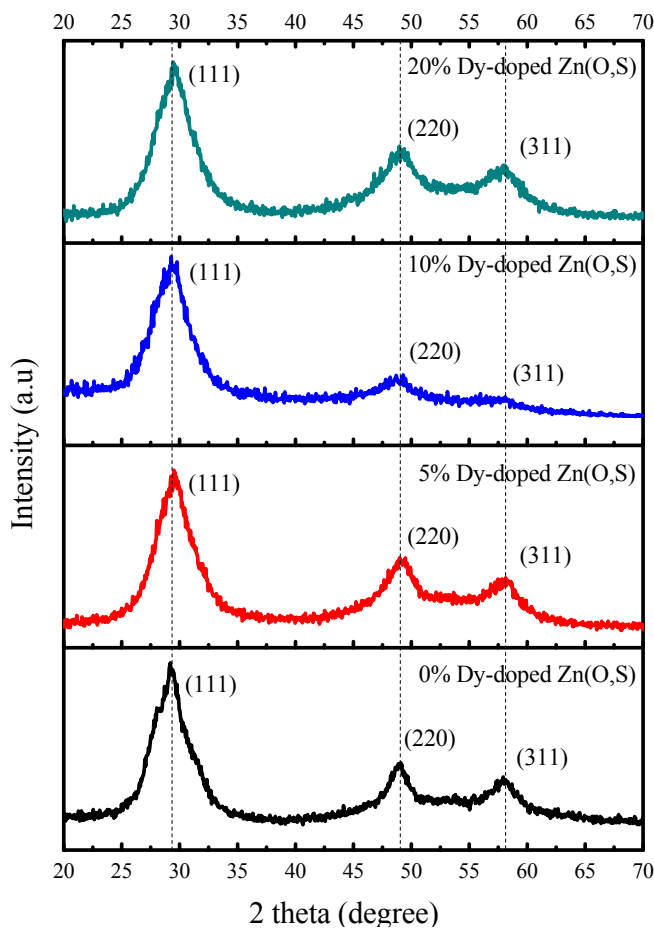


Fig. 1. XRD patterns of Dy-doped Zn(O,S) with different contents of dysprosium.

Scanning electron microscopy (SEM) analysis.

The morphology and microstructure of Dy-Zn(O,S) with different Dy contents are examined and shown in [Figure S2](#). It showed all the particles with different contents of Dy did not exhibit different morphologies. The particles less than 100 nm were aggregated to form larger agglomerates. To show all the elements in Dy-Zn(O,S)-10 NPs, FE-SEM elemental mapping was carried out on catalyst surface with a depicted-red rectangle area on the image for the mapping scan, as shown in [Fig. 2](#). The signals related with Zn, O, S, and Dy elements in Dy-Zn(O,S)-10 NPs were collected and shown as the blue, green, red, and gray dot patterns in [Fig. 2](#). The elemental mapping notified Dy had a lower signal intensity for its lower content. The amount of Dy in catalyst was confirmed with electron dispersed spectroscopy (EDS) analysis. Due to the low synthesis temperature below 100 °C, Dy amount was much lower as compared to its amount of Dy precursor. The atomic ratio values of Dy/(Zn+Dy) were 0%, 0.25%, 2.70%, and 4.20% for Dy-Zn(O,S)-0, Dy-Zn(O,S)-5, Dy-Zn(O,S)-10, and Dy-Zn(O,S)-20, respectively. The overall EDS analysis results were presented in [Table S1](#). The excessive Dy did not precipitate and was washed away during the powder preparation stage.

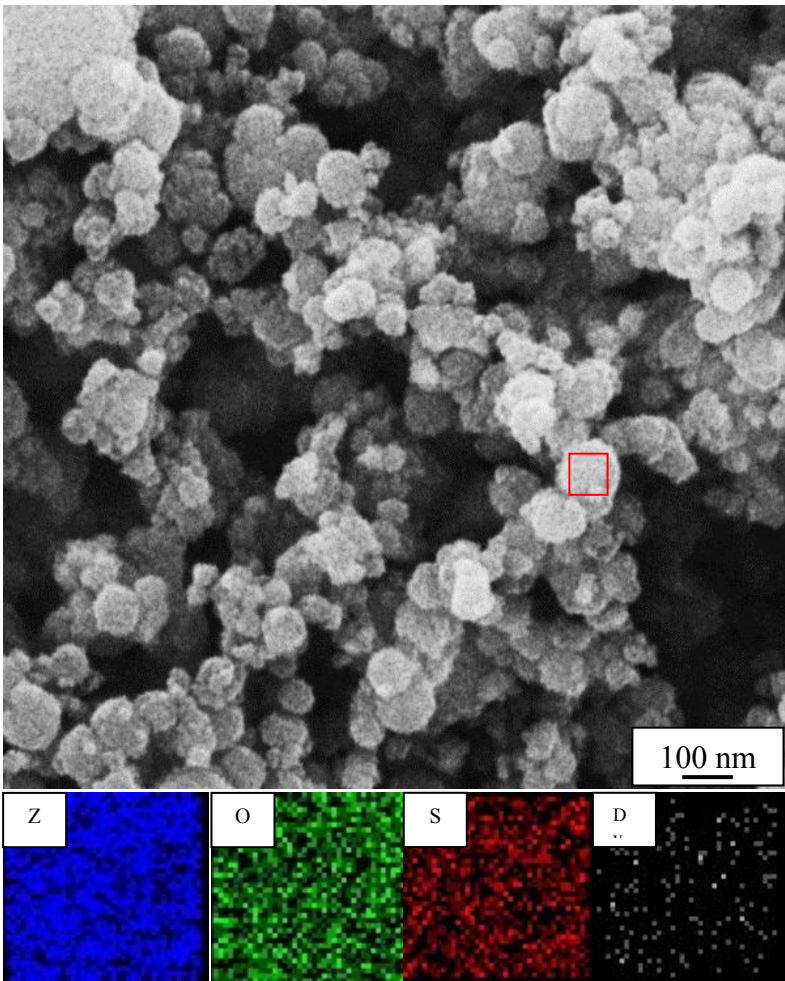


Fig. 2. SEM image of Dy-Zn(O,S)-10 nanoparticles and its elemental mapping at the depicted-red rectangle area.

Transmission electron microscopy (TEM) analysis.

[Fig. 3a](#) shows the TEM image of Dy-Zn(O,S)-10 NPs. The particle size of Dy-Zn(O,S) was very tiny and aggregated to form larger sphere-like particles with the size of 100 nm. The tiny size of Dy-Zn(O,S)-10 NPs was consistent with the crystalline size calculated with XRD data by Scherer equation. [Figs. 3b](#) and [3c](#) show the lattice fringes and selected area electron diffraction (SAED) ring patterns of Dy-Zn(O,S) NPs, respectively. The lattice fringes in [Fig. 3b](#) show the

250 lattice parameters of 2.67, 2.92, and 2.94 Å are between those of ZnO (111) and ZnS (111)
251 planes and consistent with our previous works ^{1, 11} The varying lattice fringe values in Fig. 3b
252 were related to broad ring patterns, as shown in Fig. 3c. As a broad (111) ring pattern was found,
253 the depicted-outer and -inner ring patterns corresponding with ZnO (111) and ZnS (111) planes,
254 respectively, were provided to clearly approve the formation of Dy-Zn(O,S) solid solution. The
255 broad ring patterns were also observed for (220) and (311) planes. A random distribution of the S
256 content in Dy-Zn(O,S) is the major reason for the broad diffraction ring.

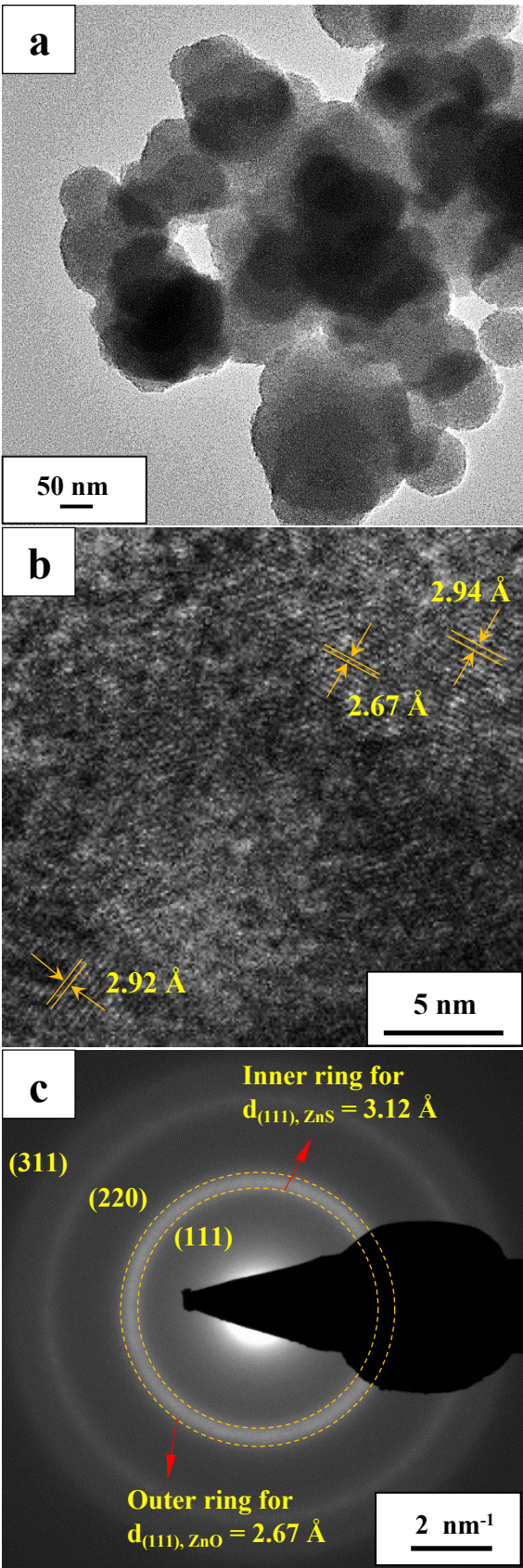


Fig. 3. (a) Low and (b) high magnification of HRTEM images of Dy-Zn(O,S)-10 with (c) the broad ring pattern obtained from SAED. The broad ring pattern for (111) was located between the depicted outer and inner ring patterns of ZnO and ZnS, indicating the formation of solid solution of oxysulfide.

Diffuse reflectance spectroscopy (DRS) analysis.

[Fig. S3a](#) show diffuse reflectance spectra of Dy-Zn(O,S) with different Dy amounts. Compared with the Dy-free Zn(O,S), all the Dy-Zn(O,S) showed an improved absorbance in the UV range. Based on the DRS measurements, the converted Tauc plots are shown in [Fig. S3b](#). Tauc plot was obtained with the formula of $\alpha h\nu = A(h\nu - E_g)^m$ for $E_g > h\nu$, where α is the material optical absorbance, $h\nu$ is the photon energy; E_g is the bandgap energy; and $m = 0.5$ and 2 are for the materials with direct and indirect allowed transition band gap, respectively. The direct bandgap values of Dy-Zn(O,S) were about 3.54–3.57 eV, which were between those of ZnO (3.2 eV) and ZnS (4.1 eV) due to the formation of solid solution. Based on the optical property data, the blacklight UV tube lamps with the wavelength of 352 nm were selected as a light source to meet the requirement for our photocatalysts.

X-ray photoelectron spectroscopy (XPS) analysis.

To identify the chemical state of each element in catalysts, XPS measurement as one of the surface-sensitive quantitative spectroscopic techniques was carried out on Dy-Zn(O,S)-10. [Fig. 4](#) shows the XPS spectra of (a) Zn 2p, (b) Dy 4d, (c) O 1s, and (d) S 2p orbitals for Dy-Zn(O,S)-10. [Fig. 4a](#) shows the binding energy values of Zn ($2p_{1/2}$) and Zn ($2p_{3/2}$) at 1046.9 eV and 1023.8 eV, respectively, which are consistent with literature data.²⁸ [Fig. 4b](#) shows the binding energy value of Dy (4d) at 152.5 eV with low energy intensity for its low content.²⁸ [Fig. 4c](#) shows the

binding energy values of O (1s) at 529.6 eV, 530.3 eV, and 531.4 eV, which are contributed from the oxygen in lattice (O_L), oxygen vacancy (O_v), and oxygen adsorbed (O_{ads}) as hydroxide, respectively, on catalyst surfaces.¹ 69.89% O_L , 15.59% O_v , and 14.52% O_{ads} were calculated from the peak area of oxygen in Fig. 4c. Fig. 4d shows the binding energy values of S ($2p_{1/2}$) and S ($2p_{3/2}$) at 164.7 eV and 163.2 eV, respectively, and were consistent with literature data.^{1, 28}

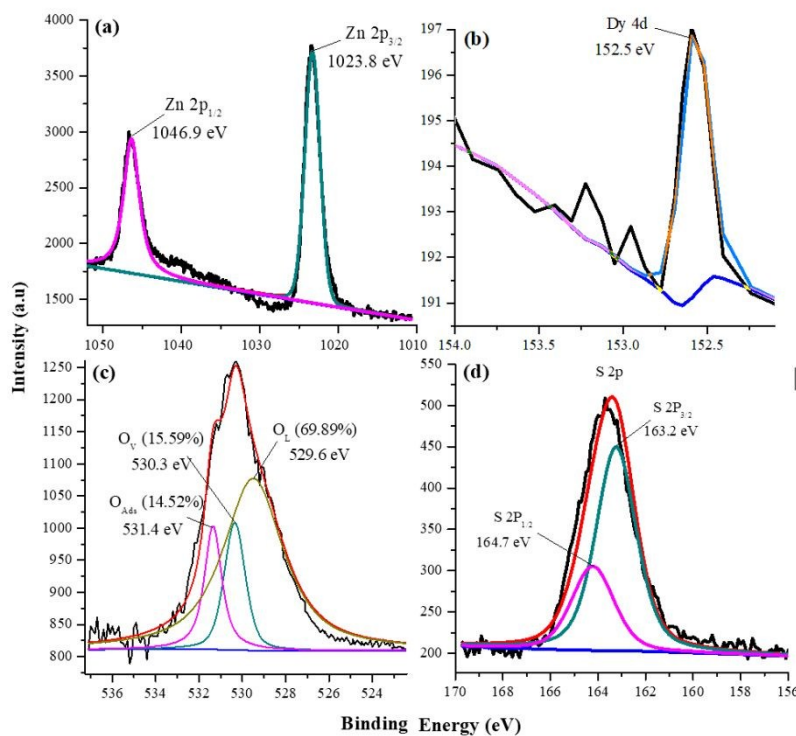


Fig. 4. XPS spectra of (a) Zn 2p, (b) Dy 4d, (c) O 1s, and (d) S 2p orbitals for Dy-Zn(O,S)-10.

Electrochemical impedance spectroscopy (EIS) analysis.

To examine the electron transfer properties of Dy-Zn(O,S) NPs with different Dy contents during photocatalytic reaction, EIS measurement was carried out in a 0.1 M KCl solution at the frequency range from 50 KHz to 0.1 Hz, window potential from -1 – 1 V, scan rate of 10 mV,

and signal amplitude of 10 mA. The catalyst-dispersed solution was prepared with 5 mg powder in 1 mL Nafion solution (DI water : isopropanol = 3 : 1) and then coated on GCE. Fig. 5 shows the electrochemical impedance spectra of Dy-Zn(O,S) with different Dy contents on a Nafion-fixed GCE electrode. The spectra were fitted with the equivalent Randles circuit to obtain the resistance values of 34.2 K Ω , 14.9 K Ω , 6.56 K Ω , and 21.4 K Ω for Dy-Zn(O,S)-0, Dy-Zn(O,S)-5, Dy-Zn(O,S)-10, and Dy-Zn(O,S)-20, respectively. Dy-Zn(O,S)-10 with 6.56 K Ω showed the lowest resistance, indicating the most efficient electron transfer property at the interface between electrode and electrolyte during the EIS measurement. From the experimental data, Dy-Zn(O,S)-10 is expected to have the excellent photocatalytic activity.

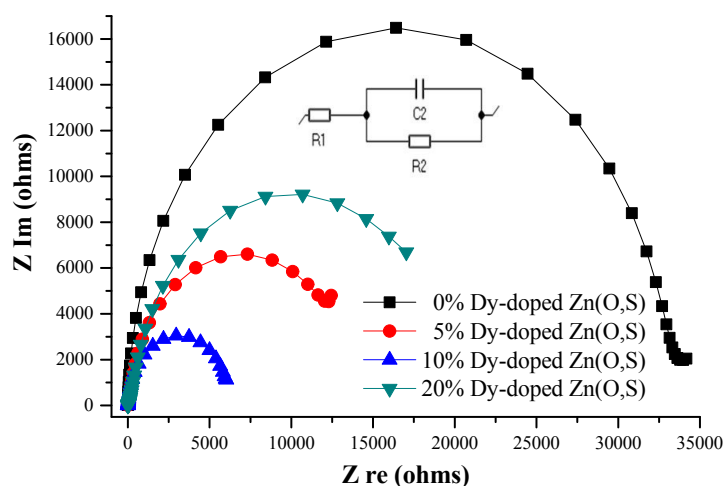


Fig. 5. Electrochemical impedance spectra of Dy-Zn(O,S) with different Dy contents on a Nafion-fixed GCE electrode in 0.1 M KCl solution. The inset shows the equivalent Randles circuit for curve fitting.

Photoresponse analysis.

One of the indications for photocatalytic activity is the photocurrent induced by photon during light illumination. If a higher current is induced by photon, a higher catalytic activity can occur to support HER or hydrogenation reaction. Fig. 6 shows the photoresponses of Dy-Zn(O,S) at different Dy contents on modified GCE as working electrodes in 0.1 M KCl solution under UV LED light illumination with the chopping frequency of 25 mHz. The photo current values were measured to be 102, 117, 192, and 136 pA for Dy-Zn(O,S)-0, Dy-Zn(O,S)-5, Dy-Zn(O,S)-10, and Dy-Zn(O,S)-20, respectively. Dy-Zn(O,S)-10 achieved the highest photo current of 192 pA. The other feature in Fig. 6 is the longer tail for the Dy-Zn(O,S)-10, which indicates a slower recombination rate between hole and electron after the light illumination is turned off. The photo current data was also consistent with EIS data in Fig. 5.

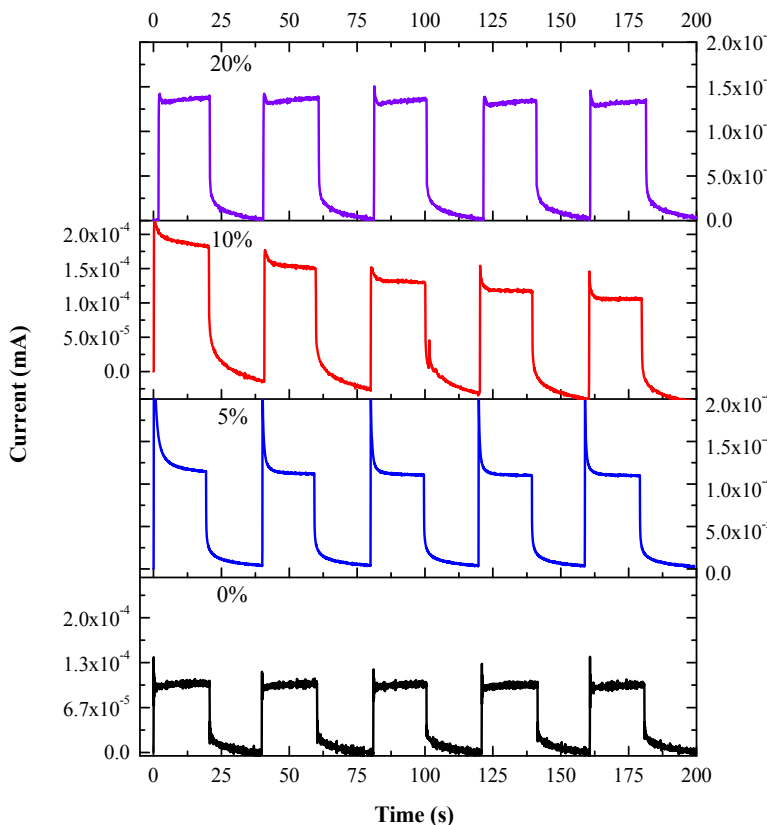


Fig. 6. Photoresponses of Dy-Zn(O,S) with different Dy contents on a Nafion-fixed GCE working electrode in 0.1 M KCl solution under UV LED light illumination with a chopping frequency of 25 mHz.

Assessment of photocatalytic HER.

Fig. 7 shows the amounts of hydrogen evolved from 10% ethanol solution with different Dy-Zn(O,S) catalysts. The experimental data indicated Dy-Zn(O,S) prepared with different Dy precursor contents of 0, 5, 10, and 20% could achieve 25.8, 37.6, 40.8, and 31.1 mmol/g, respectively, for 5 h photocatalytic reaction. The maximum amount of evolved hydrogen reached 40.8 mmol/g or 8.160 mmol/g·h, which was significantly enhanced by almost 60%, as compared to that with Dy-free Zn(O,S).¹ The color of Dy-Zn(O,S) powders were changed to gray color during the HER reaction but reversibly changed back. This phenomenon supports the reversible process with the lattice oxygen removal for oxygen vacancy at the light-on condition and the annihilation of oxygen vacancy at the light-off condition.

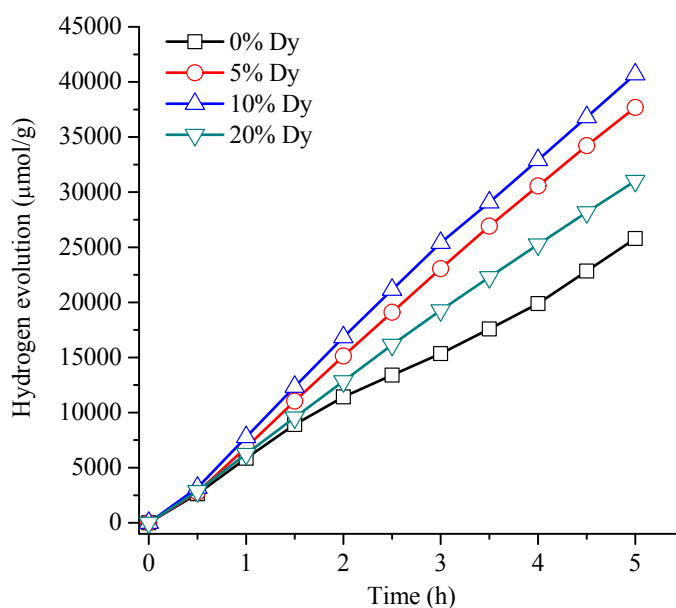


Fig. 7. Hydrogen evolution amounts from a 10% ethanol solution in the presence of Dy-Zn(O,S) with different Dy contents under blacklight UV tube lamps illumination.

Evaluation of photocatalytic hydrogenation of 4-NP to 4-AP.

After the evaluations with EIS, photoresponse, and HER, Dy-Zn(O,S)-10 was selected for green chemical conversion. Fig. 8 shows the variation of UV-vis spectra with reaction time for 30 ppm 4-NP catalyzed with (a) Na_2SO_3 +Dy-Zn(O,S)-10, (b) Na_2SO_3 +Zn(O,S), and (c) Dy-Zn(O,S)-10 after illuminated with $4\text{ W} \times 4$ UV blacklight tube lamps. Fig. 8a shows the total conversion of NP to nitrophenolate with a characteristic peak at 400 nm for Dy-Zn(O,S) in the presence of sulfite ions. The nitrophenolate ions gradually converted to 4-AP in 45 min, accompanied with the disappearance of peak at 400 nm and the appearance of peaks at 302 and 230 nm. Fig. 8b shows the chemical conversion with Dy-free Zn(O,S). It displayed a similar conversion behavior to that with Dy-doped one but took more than 60 min to complete the conversion. The data indicated Dy doping also improved the photocatalytic activity of Zn(O,S) for chemical conversion of 4-NP. The absorbance at 400 nm in UV-vis spectra is due to the formation of nitrophenolate ions after adding Na_2SO_3 . As the solution pH becomes higher, nitrophenolate ions will be formed and adsorbed on catalyst surfaces, subsequently, the absorbance peak at 400 nm becomes lower for Dy-doped Zn(O,S). The data suggests more positively oxygen-vacancy-sites of Dy-doped Zn(O,S) have more adsorption of negatively nitrophenolate ions as compared to Dy-free Zn(O,S), therefore the reduction of nitrophenol on Dy-doped Zn(O,S) is faster. Fig. 8c shows the chemical conversion of 4-NP without the addition of Na_2SO_3 . Here, there was no nitrophenolate peak at 400 nm before the light illumination. The conversion from 4-NP with peak at 317 nm occurred slowly not only to 4-AP with peaks at 302 and 230 nm but also to nitrophenolate with peak at 400 nm. Therefore, 4-NP could be well reduced to 4-AP with Dy-

Zn(O,S)-10 in Na₂SO₃ solution at a relatively short time. After the conversion, the powder was evaluated with XRD to study its structural stability. As shown in Fig. S4, no observable structural change can be detected. Other *M*-Zn(O,S) photocatalysts with *M*= Sn, Mn, and La had been evaluated, however a twice conversion time was needed.^{9, 29, 30} Therefore, it is one of the purposes to use the excellent Dy-Zn(O,S) for conversion of azobenzene to aniline, which is commonly known as a sluggish conversion reaction.

The 4-NP-to-4-AP conversion was further analyzed with HPLC. 4-NP and 4-AP were respectively monitored with UV and fluorescent detectors at the retention times of 31.8 min and 18.3 min. Fig. S5 shows HPLC plots of (a) 4-NP and (b) 4-AP solutions after photocatalytic reduction in the presence of Dy-Zn(O,S)-10. The conversion was complete in 2 h with the gradual increased peak intensity of 4-AP and the gradually decreased intensity of 4-NP.

To understand the kinetic mechanism of 4-NP reduction, the experiments to observe the evolved hydrogen with and without 30 ppm 4-NP solution in the presence of Dy-Zn(O,S)-10 and Na₂SO₃ were executed with GC-TCD. Fig. S6 shows the amounts of evolved hydrogen during the photocatalytic session in the presence of Dy-Zn(O,S)-10 with and without 4-NP in solution. The data showed the amount of the evolved hydrogen in 4-NP solution was lower than that in 4-NP-free solution, implying the evolved hydrogen ions on catalyst were not reduced by electron to form hydrogen gas, but used for the reduction of 4-NP to 4-AP.

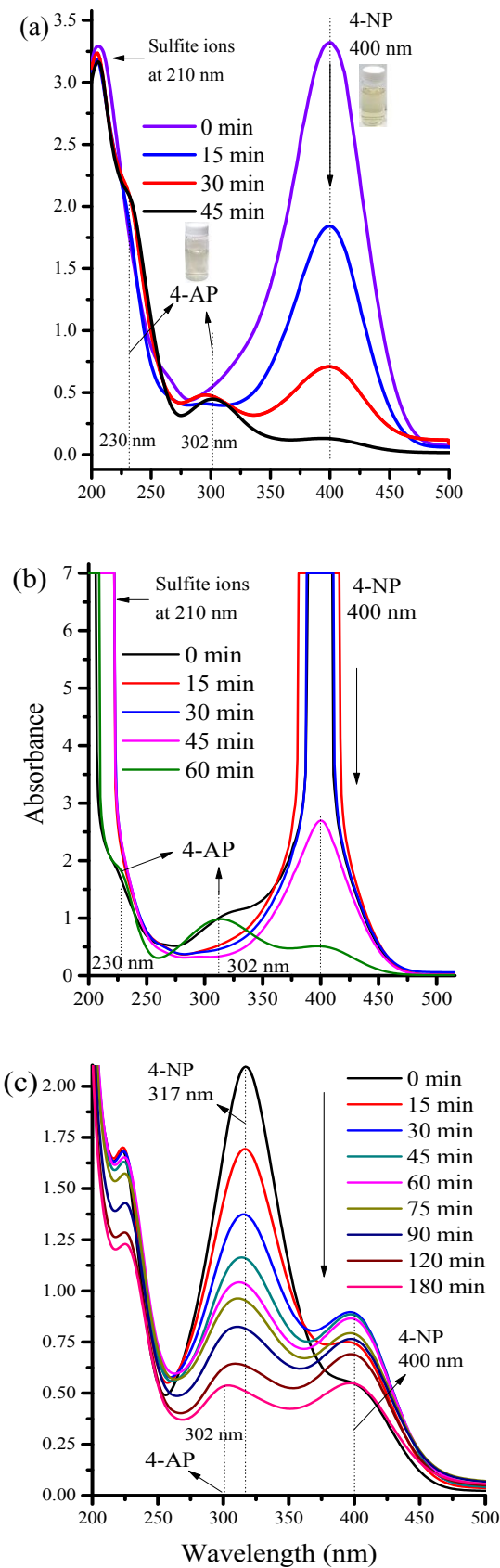


Fig. 8. The variation of UV-vis spectra with reaction time for 30 ppm 4-NP catalyzed with (a) $\text{Na}_2\text{SO}_3 + \text{Dy-Zn(O,S)-10}$, (b) $\text{Na}_2\text{SO}_3 + \text{Zn(O,S)}$, and (c) Dy-Zn(O,S)-10 after illuminated with $4 \text{ W} \times 4 \text{ UV}$ blacklight tube lamps.

Evaluation of photocatalytic hydrogenation of azobenzene to aniline.

Fig. 9a shows the UV absorbance spectra of 15 ppm azobenzene solution after 0-min, 15-min, 30-min, and 60-min photo reaction with Dy-Zn(O,S)-10 . As the trans-azobenzene easily changed to cis-azobenzene under light (UV or vis) illumination, the specific absorbance spectrum of cis-azobenzene was observed before light illumination for PHR. After 15-min photo reaction, the UV absorbance peaks of AB were shifted to the characteristic peaks of aniline at 237 nm. 48% aniline was formed in 15 min from AB, after we compared it with the peak intensity of 15 ppm standard aniline at the same condition. An appropriate hydrogenation reaction step is proposed and shown as an inset in **Fig. 9a**. To ensure the formation of aniline as a hydrogenation product, the other experiment with higher concentration of 60 ppm azobenzene was carried out and the aliquots after 0-h, 2-h, 4-h, and 6-h reactions were taken for GC-MS measurement. The result of GC-MS measurement after 6 h reaction was shown in **Fig. 9b** and it revealed that 60 ppm azobenzene was totally converted to aniline after 6-h reaction. Although the UV-vis spectra data indicated about 48% of the azobenzene had been hydrogenated to aniline in 15 min, however to achieve 100 % azobenzene-hydrogenated aniline, a relatively lengthy photocatalytic session was required. It might be due to the much higher AB concentration or the converted aniline on catalyst to cover the active sites of catalyst. The existences of azobenzene and aniline during 2 h, 4 h, and 6 h reactions were shown in the inset in **Fig. 9b**. During the photocatalytic conversion reaction at 2 h and 4 h, azobenzene and aniline were still existed in solution. However, after 6-h reaction, only aniline was detected as a product of azobenzene hydrogenation. Commonly,

hydrogenation reaction for chemicals with azo bond is quite hard, however the experimental data indicate that the double bond of nitrogen in azobenzene could be broken and hydrogenated with Dy-Zn(O,S) photocatalyst. To show the effect of Dy doping, pure Zn(O,S) (without Dy doping) was used to hydrogenate azobenzene with the same experimental condition. The result indicated pure Zn(O,S) could not totally convert azobenzene to aniline as one of the characteristic cis-azobenzene peaks at 430 nm in UV-vis measurement (Fig. S7) was still shown up, which revealed intermediates might remain for Dy-free Zn(O,S) catalyst. To show a hydrogenation reaction to use the hydrogen generated from HER on Dy-Zn(O,S), an experiment to measure the evolved hydrogen with and without azobenzene was conducted for the solution. Fig. S8 shows the hydrogen evolution obtained from HER on Dy-Zn(O,S)-10 nanoparticles with and without 60 ppm azobenzene in 10% ethanol solution. It was obviously shown that the evolved hydrogen amount from azobenzene-contained solution was lower than that from azobenzene-free solution. After the conversion, the powder was evaluated with XRD to study its structural stability. As shown in Fig. S9, no observable structural change can be detected.

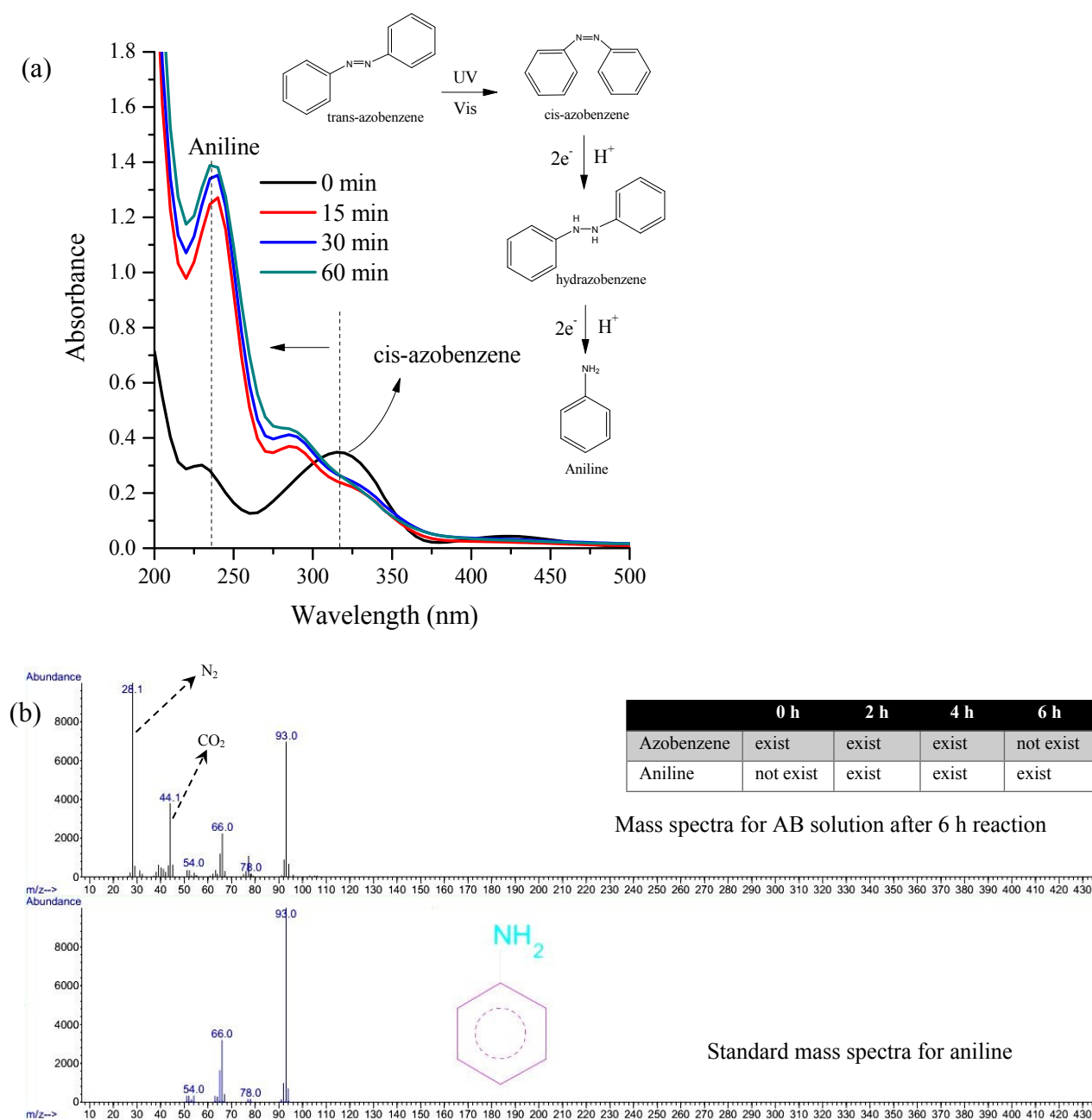
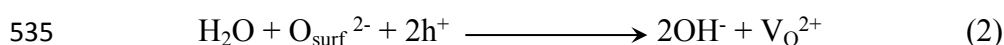
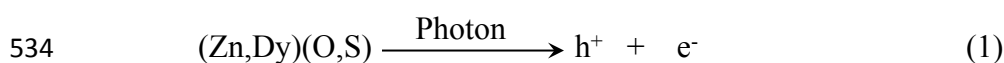


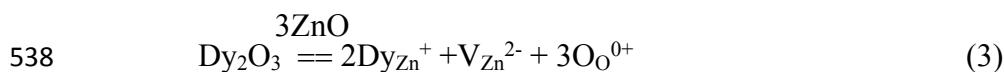
Fig. 9. (a) UV-vis absorbance spectra of 15 ppm azobenzene solution with different photo reaction times and (b) GC-MS spectra of 60 ppm azobenzene solution after 6 h reaction with a inset table to show the existences of azobenzene and aniline in different reaction times.

523 Photocatalytic hydrogenation mechanism

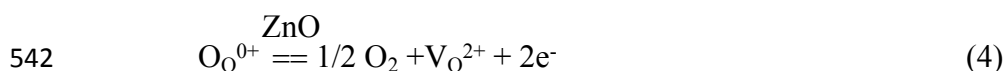
524 The basic reaction steps for PHR needs to be consistent HER. Based on the experimental data
 525 which showed the solution color reversibly changed, PHR is expected to be initiated with the
 526 water oxidation to form oxygen vacancy which further reduces water to form H^+ ions. As the H^+
 527 ions are available on catalyst surface, there are two possibilities for it, either to form hydrogen
 528 gas or to undergo hydrogenation reaction. For Dy-Zn(O,S), the photocatalytic reactions are
 529 proposed and presented with the Kröger–Vink notation³¹ for defects. As Dy-Zn(O,S) catalyst is
 530 illuminated with UV light, electron and hole are generated on conduction and valence bands,
 531 respectively, as shown in Eq. (1). The generated hole will oxidize water with the assistance of
 532 active surface oxygen to form hydroxide and positively-charged oxygen vacancy, as indicated in
 533 Eq (2).^{1, 7, 11-13, 31}



536 The formation of active surface oxygen is evaluated for the next paragraphs. Dy-doped Zn(O,S)
 537 can have the defect equation expressed below:



539 However, Dy-Zn(O,S) had lower electrical resistance than the Dy-free Zn(O,S), as shown in Fig.
 540 5. To support the evidence in electrical resistance, the defect equation in Zn(O,S) for oxygen
 541 vacancy together with electrons is listed in Eq. (4) below.



Together with the intrinsic Schottky defect equation of Eq. (5): $\text{null} = V_{\text{Zn}}^{2-} + V_{\text{O}}^{2+}$, the Dy-Zn(O,S) has the overall defect reaction in Eq. (6) below:



The Dy-on-Zn defect is a donor one to increase electron concentration and low electrical resistance, as shown in Fig. 5. Therefore, the Dy doping is to lower electrical resistance with the electron contribution in Eq. (6). Based upon the equilibrium constant of Eq. (4), the higher e^- concentration leads to the lower $[V_{\text{O}}^{2+}]$. For the Dy-free Zn(O,S), on the other hand, the defect equation (7): $1/2 \text{O}_2 + 2\text{e}^- = V_{\text{Zn}}^{2-} + \text{O}_{\text{O}}^{0+}$, is achieved by subtracting Eq. (4) from Eq. (5). This mechanism involves the electron elimination to lead Zn(O,S) with high electrical resistance, as supported with Fig. 5. Based upon the equilibrium constant of Eq. (7), the lower e^- concentration for Dy-free Zn(O,S) leads to the lower $[V_{\text{Zn}}^{2-}]$ or higher $[V_{\text{O}}^{2+}]$. With the interaction between point defect and surface/interface, Eq. (8) and Eq. (9) below have to be kept.

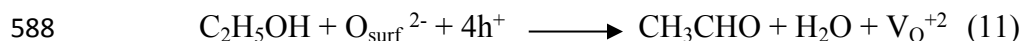


As observed in Table S2 in supplementary data, the Dy-free Zn(O,S) has a higher V_{O}^{2+} content, but $[V_{\text{O}}^{2+}]$ is lower with the addition of Dy. That is $[V_{\text{O}}^{2+}]_{\text{Dy-free}} > [V_{\text{O}}^{2+}]_{\text{Dy}}$, so $[\text{O}_{\text{surf}}^{2-}]_{\text{Dy-free}} < [\text{O}_{\text{surf}}^{2-}]_{\text{Dy}}$ based upon Eq. (9) can be obtained. The meaning for $[\text{O}_{\text{surf}}^{2-}]_{\text{Dy-free}} < [\text{O}_{\text{surf}}^{2-}]_{\text{Dy}}$ is that Dy-Zn(O,S) has more negatively charged surface oxygen ions than Dy-free Zn(O,S). The more negatively charged catalyst is expected to have stronger interaction with other chemicals through Eq. (2). The interaction between defect and interface becomes severe, when the particle size becomes small with a small radius of curvature. Therefore, more active surface oxygen ions occur on Dy-Zn(O,S), as compared with Dy-free Zn(O,S).

After the active surface oxygen-involved water oxidation in Eq. (2), the oxygen vacancy sites then can trap water molecule to form the adsorbed H₂O and to weaken its O-H bond. This interaction between adsorbed water and oxygen vacancy site on catalyst surface finally generates hydrogen ions, as shown in Eq. (10). Without the 4-NP and AB, the proton in Eq. (10) is used for the HER mechanism.⁹ With 4-NP, Na₂SO₃ has been added to act not only as an electron transfer mediated agent for forming nitrophenolate ion,³² but also as the hole scavenger to be oxidized by photo generated hole to SO₃^{•-} radical. The schematic diagram for the kinetic mechanism for PHR of 4-NP is shown in Fig. S10, where the reaction steps demonstrate the continuous hydrogenation reactions with the aids of protons and electrons.



To be consistent with our proposed mechanism for HER and the 4-NP conversion, the initiation of photocatalytic AB-to-aniline conversion must involve Eqs. (1) – (3) for producing proton, electron, and active surface oxygen. For the AB-to-aniline conversion, the addition of ethanol is not only important for the dissolution of AB in water but also useful to act as a hole scavenger to initiate Eq. (11) below for generating important species of oxygen vacancy and lowering the hole concentration. The oxygen vacancy needs to interact with H₂O for protons and with AB for the pinning of its N in the N=N bond. Although Dy-Zn(O,S) is expected to have more active surface oxygen ions due to $[\text{O}_{\text{surf}}^{2-}]_{\text{Dy-free}} < [\text{O}_{\text{surf}}^{2-}]_{\text{Dy}}$, too much Dy-doping content to form too much oxygen vacancy is not beneficial because of the lattice relaxation to weaken the interaction with H₂O or azobenzene. An optimal Dy content in Zn(O,S) is required to achieve the best reaction condition. The schematic diagram for the kinetic mechanism for the PHR of azobenzene is shown in Fig. 10. The pinned c-AB goes through continuous PHR with the available protons and electrons to form aniline.



589 The strong adsorption of azobenzene on Dy-Zn(O,S) is the crucial step for fast PHR.
590 According to the experimental data in Fig. S11, about 50% of 15 ppm azobenzene can be
591 adsorbed on catalyst during stirring process without light illumination. This adsorption can be
592 attributed to the columbic interaction of the negatively charge Dy-Zn(O,S) with the electron-
593 deficient N=N bonds of AB, while keeping the electron-rich benzyl groups away from catalyst. It
594 is assumed that AB is attracted toward catalyst, followed by the AB pinning at the oxygen
595 vacancy. The chemicals to be reduced not only need to have water solubility but also the
596 adsorptive behavior on catalyst to have intimate contacts and prolonged surface retention time
597 for surface reactions to occur. Here, a 48% conversion of 15 ppm azobenzene to aniline in 15
598 min or a 100% conversion of 60 ppm AB to aniline in 6 h had been carried out, as shown in Fig.
599 9.

600 As visible-light-driven photocatalyst has been widely promoted for its efficient utilization
601 under solar light, our UV-light-driven one operated under the much lower light power density of
602 1/40 sun light remains promising.¹ In our system, there is no need of water cooling for our
603 chemical conversion system to avoid the vaporization of chemicals and solvents. We did not use
604 Pt and Au noble metals, which have to be applied on TiO₂ in order to generate a sufficient
605 amount of H₂ for hydrogenation reactions. The reversible and activated surface oxygen/oxygen
606 vacancy exchange kinetic mechanism supports our fast HER. We prepared the catalyst below
607 100 °C without using surfactants to achieve catalyst with the active surface oxygen for initiating
608 PHR under light illumination.

609 The progress from photocatalytic HER to green chemical conversion needs to be considered
610 together. The condition for a photocatalyst to achieve a better green chemical conversion on
611 photocatalytic reduction of azobenzene to aniline needs to have a better HER production rate for
612 the purpose of generating protons. From the basic kinetics of HER, the best photocatalyst with
613 the fastest H_2 formation from the H adatoms might not be the best choice for chemical
614 conversion due to the fast consumption of protons, but catalyst without sufficient H_2 amount
615 cannot do the chemical conversion. A suitable retention time for both of the chemicals and the
616 adsorbed H^+ ions or H adatoms on catalyst surface to involve the surface chemical reaction is
617 necessary. With the partial coverage of catalyst by chemicals for PHR, the un-covered catalyst
618 surface always has to undergo HER. Therefore, the slower HER rate of 5.16 mmol/g·h for Dy-
619 free Zn(O,S) in Fig. 7, as compared to 8.16 mmol/g·h for Dy-Zn(O,S)-10 one, leads to a much
620 slower chemical conversion of 4-NP (Fig. 8b) and an incomplete conversion of AB (Fig. S8).
621 Our data suggest that catalyst with a higher HER rate implies a catalyst with high PHR activity.
622 PHR is not recommended for using photocatalyst with a HER rate less than 5 mmol/g·h. As HER
623 rate is related to the catalysts, solvent, co-solvent, hole scavenger, light source etc,^{6,7} the solvent
624 solubility for AB here, the interaction between AB and catalyst, the interaction of reaction
625 products with catalyst, etc. can change the HER kinetics for protons. Any inconsistent reaction
626 condition for PHR with the proven HER can greatly diminish the availability of the surface
627 protons and the H adatoms. Here, ethanol in our aqueous system is not only the best-chosen hole
628 scavenger to reach the highest HER rate but also the good solvent for AB. Therefore, the
629 chemical conversions here are stick to the ethanol/water solvent system used for our best HER.
630 With the further help of AB adsorption of ~50% on catalyst, the PHR with N=N bond cleavage
631 for aniline can be achieved.

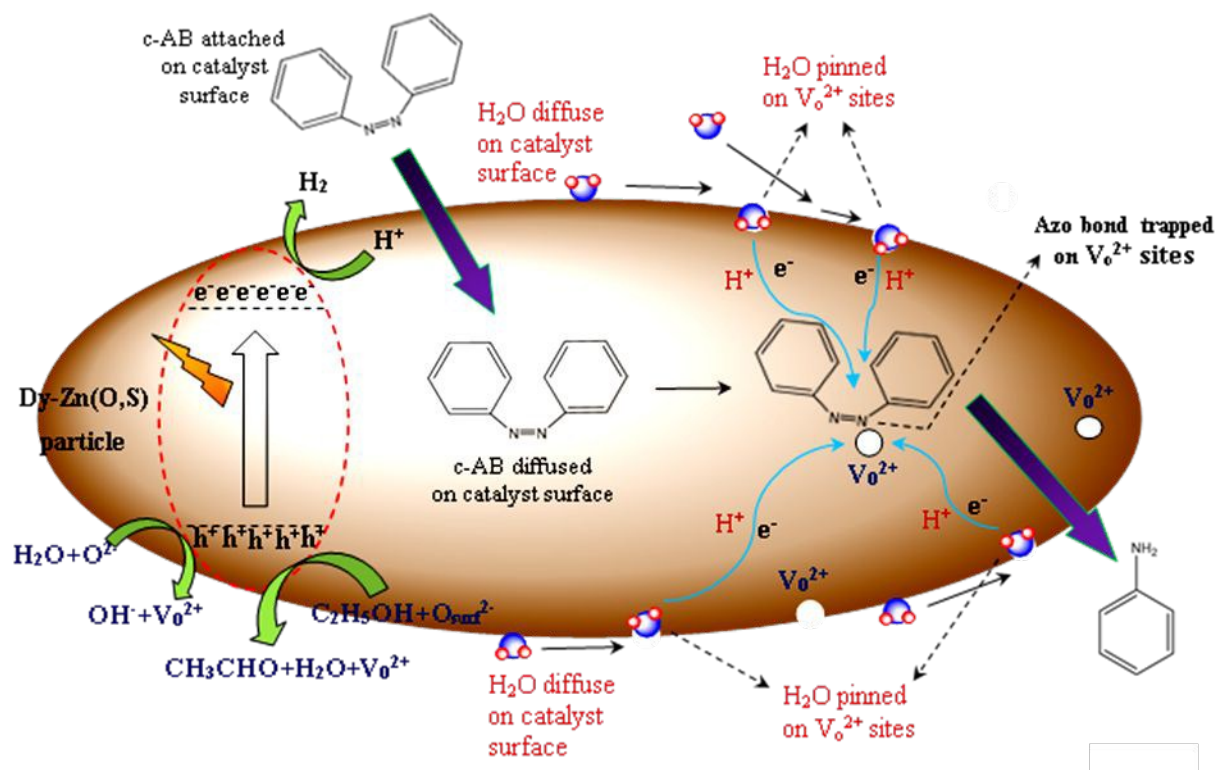


Fig. 10. Schematic mechanism of azobenzene hydrogenation in the presence of Dy-Zn(O,S)-10 nanoparticle under low intensity of UV light illumination.

The mechanism in hydrogenation azobenzene (AB) is critical. As the oxygen vacancy sites were formed during the photocatalytic reaction, the positively oxygen vacancy sites would trap negatively double-bond nitrogen. The further steps of hydrogenation of double-bond nitrogen would subsequently occur on catalyst surface, since the immobilized AB which was stuck on catalyst surface was an advantage for complete hydrogenation of AB to aniline, instead of hydrazobenzene as intermediate. The overall reaction illustration was provided in Fig. 10.

Conclusions

Dy-doped Zn(O,S) photocatalysts had been prepared with different amounts of Dy precursors to obtain the Dy-Zn(O,S)-10 with the lowest charge transfer resistance of 6.56 k Ω , the strongest photoresponse of 192 pA, and the highest hydrogen production rate of 8.16 mmol/g·h. The proton and electron used for photocatalytic hydrogen evolution was attempted for photocatalytic hydrogenation reactions of nitrophenol to aminophenol and azobenzene to aniline. We were successful with the 100% conversion of 30 ppm NP to AP in 45 min with Na₂SO₃ as hole scavenger under low power UV illumination. We also succeeded in reducing 100% azobenzene of 60 ppm to aniline in 6 h with 10% ethanol as hole scavenger. This work proves the requirement of using good hydrogen-evolved photocatalyst for fast hydrogenation reactions. The proposed kinetic mechanism involves the active surface oxygen on Dy-Zn(O,S), based upon the phenomenon of reversible color change and supported with the kinetic point defect model. N=N bond cleavage for fully converting azobenzene to aniline involves the steps of solvation, adsorption, pinning, and surface hydrogenation reaction in sequence. At this stage, the 100% conversion of azobenzene to aniline in 6 h with the N=N bond cleavage at mild condition gives a promising example for green chemistry.

660

661 ACKNOWLEDGMENTS

This work was supported by the Ministry of Science and Technology of Taiwan under Grant numbers MOST 107-2811-E-011-008 and MOST 107-2221-E-011-141-MY3.

664

665 REFERENCES

- 666 1. H. Abdullah, D.-H. Kuo and X. Chen, *International Journal of Hydrogen Energy*, 2017,
667 **42**, 5638-5648.
- 668 2. A. Kudo and Y. Miseki, *Chemical Society Reviews*, 2009, **38**, 253-278.
- 669 3. M. Reza Gholipour, C.-T. Dinh, F. Béland and T.-O. Do, *Nanoscale*, 2015, **7**, 8187-8208.
- 670 4. K. Maeda, *Journal of Photochemistry and Photobiology C: Photochemistry Reviews*,
671 2011, **12**, 237-268.
- 672 5. B. Gupta, A. A. Melvin, T. Matthews, S. Dash and A. K. Tyagi, *Renewable and*
673 *Sustainable Energy Reviews*, 2016, **58**, 1366-1375.
- 674 6. H. Ahmad, S. K. Kamarudin, L. J. Minggu and M. Kassim, *Renewable and Sustainable*
675 *Energy Reviews*, 2015, **43**, 599-610.
- 676 7. H. Abdullah, N. S. Gultom, D.-H. Kuo and A. D. Saragih, *New Journal of Chemistry*,
677 2018, DOI: 10.1039/C7NJ05124G.
- 678 8. H. Tada, T. Ishida, A. Takao and S. Ito, *Langmuir*, 2004, **20**, 7898-7900.
- 679 9. G. Noto Susanto, A. Hairus and K. Dong-Hau, *Journal of Physics: Conference Series*,
680 2018, **1007**, 012061.
- 681 10. F. Mahdavi, T. C. Bruton and Y. Li, *The Journal of Organic Chemistry*, 1993, **58**, 744-
682 746.
- 683 11. H. Abdullah, N. S. Gultom and D.-H. Kuo, *New Journal of Chemistry*, 2017, **41**, 12397-
684 12406.
- 685 12. N. S. Gultom, H. Abdullah and D.-H. Kuo, *International Journal of Hydrogen Energy*,
686 2017, **42**, 25891-25902.
- 687 13. N. S. Gultom, H. Abdullah and D.-H. Kuo, *Journal of the Energy Institute*, 2018, DOI:
688 <https://doi.org/10.1016/j.joei.2018.08.008>.

- 689 14. A.-M. Alexander and J. S. J. Hargreaves, *Chemical Society Reviews*, 2010, **39**, 4388-
690 4401.
- 691 15. C. Avelino, C. Patricia and S. Pedro, *Angewandte Chemie International Edition*, 2007,
692 **46**, 7266-7269.
- 693 16. M. Boronat, P. Concepción, A. Corma, S. González, F. Illas and P. Serna, *Journal of the*
694 *American Chemical Society*, 2007, **129**, 16230-16237.
- 695 17. A. Corma, P. Serna, P. Concepción and J. J. Calvino, *Journal of the American Chemical*
696 *Society*, 2008, **130**, 8748-8753.
- 697 18. A. Corma and P. Serna, *Science*, 2006, **313**, 332-334.
- 698 19. B. Saha, S. De and S. Dutta, *Critical Reviews in Environmental Science and Technology*,
699 2013, **43**, 84-120.
- 700 20. J. Wang, Z. Yuan, R. Nie, Z. Hou and X. Zheng, *Industrial & Engineering Chemistry*
701 *Research*, 2010, **49**, 4664-4669.
- 702 21. H. Li, Q. Zhao, Y. Wan, W. Dai and M. Qiao, *Journal of Catalysis*, 2006, **244**, 251-254.
- 703 22. S.-P. Lee and Y.-W. Chen, *Journal of Molecular Catalysis A: Chemical*, 2000, **152**, 213-
704 223.
- 705 23. H.-y. Jiang, J. Xu and B. Sun, *Applied Organometallic Chemistry*, 2018, **32**, e4260.
- 706 24. N. Daems, J. Wouters, C. Van Goethem, K. Baert, C. Poleunis, A. Delcorte, A. Hubin, I.
707 F. J. Vankelecom and P. P. Pescarmona, *Applied Catalysis B: Environmental*, 2018, **226**,
708 509-522.
- 709 25. G. Xiao, P. Li, Y. Zhao, S. Xu and H. Su, *Chemistry – An Asian Journal*, 2018, **13**, 1950-
710 1955.

- 711 26. H. Tada, M. Kubo, Y. Inubushi and S. Ito, *Chemical Communications*, 2000, DOI:
712 10.1039/B001062F, 977-978.
- 713 27. Y. Shiraishi, M. Katayama, M. Hashimoto and T. Hirai, *Chemical Communications*,
714 2018, **54**, 452-455.
- 715 28. J. Moulder, W. Stickle, P. Sobol and K. Bomben, *Handbook of X-ray Photoelectron*
716 *Spectroscopy*, Physical Electronics, Inc., 1981.
- 717 29. H. Abdullah and D.-H. Kuo, *International Journal of Hydrogen Energy*, 2018, DOI:
718 <https://doi.org/10.1016/j.ijhydene.2018.04.036>.
- 719 30. H. Abdullah, N. Susanto Gultom and D.-H. Kuo, *Journal of Hazardous Materials*, 2019,
720 **363**, 109-118.
- 721 31. Y.-M. Chiang, D. P. Birnie III and W. D. Kingery, John Wiley & Sons, 1997.
- 722 32. A. Hernández-Gordillo, A. G. Romero, F. Tzompantzi and R. Gómez, *Applied Catalysis*
723 *B: Environmental*, 2014, **144**, 507-513.
- 724